RAPID COMMUNICATIONS IN MASS SPECTROMETRY
*Rapid Commun. Mass Spectrom.* 2010; **24**: 2591–2604
Published online in Wiley InterScience (www.interscience.wiley.com) DOI: 10.1002/rcm.4671

RCM

# Role of 2-oxo and 2-thioxo modifications on the proton affinity of histidine and fragmentation reactions of protonated histidine†

**Adrian K. Y. Lam[1,2,3], Craig A. Hutton[1,2] and Richard A. J. O'Hair[1,2,3]***

[1]School of Chemistry, The University of Melbourne, Victoria 3010, Australia
[2]Bio21 Institute of Molecular Science and Biotechnology, The University of Melbourne, Victoria 3010, Australia
[3]ARC Centre of Excellence for Free Radical Chemistry and Biotechnology

Received 17 May 2010; Revised 14 June 2010; Accepted 14 June 2010

**A combination of electrospray ionisation (ESI), multistage and high-resolution mass spectrometry experiments was used to compare the gas-phase chemistry of the amino acids histidine (1), 2-oxo-histidine (2), and 2-thioxo-histidine (3). Collision-induced dissociation (CID) of all three different proton-bound heterodimers of these amino acids led to the relative gas-phase proton affinity order of: histidine >2-thioxo-histidine >2-oxo-histidine. Density functional theory (DFT) calculations confirm this order, with the lower proton affinities of the oxidised histidine derivatives arising from their ability to adopt the more stable keto/thioketo tautomeric forms. All protonated amino acids predominately fragment via the combined loss of $H_2O$ and CO to yield $a_1$ ions. Protonated 2 and 3 also undergo other small molecule losses including $NH_3$ and the imine $HN{=}CHCO_2H$. The observed differences in the fragmentation pathways are rationalised through DFT calculations, which reveal that while modification of histidine via the introduction of the oxygen atom in 2 or the sulfur atom in 3 does not affect the barriers against the loss of $H_2O$+CO, barriers against the losses of $NH_3$ and $HN{=}CHCO_2H$ are lowered relative to protonated histidine. Copyright © 2010 John Wiley & Sons, Ltd.**

Post-translational modification (PTM) of a protein alters its chemical and physical properties. More importantly, PTMs can influence the biological function of a protein. An important example is oxidation of proteins by reactive oxygen species (ROS), which is implicated in aging and oxidative stress. Since oxidation changes the mass of a protein, mass spectrometry can be used to search for modified peptides or proteins as diagnostic markers of pathological conditions.[1] Amino acid residues that are readily susceptible to oxidation include the sulfur-containing amino acid residues cysteine and methionine as well as those containing an aromatic side chain, such as tyrosine, tryptophan and histidine, **1**. Oxidation of cysteine, methionine, tyrosine and tryptophan residues has been shown to influence the gas-phase chemistry of protonated amino acids and peptides.[2–10] For example, methionine sulfoxide residues give a diagnostic side-chain loss of $CH_3SOH$.[5,11–13]

Although the susceptibility of histidine (**1**) (Scheme 1) and histidine residues towards metal-catalysed oxidation is well known,[14] and can be a competing reaction in 'click' chemistry bioconjugation strategies,[15] only recently has there has been evidence to support the idea that stable histidine oxidation products such as 2-oxo-histidine (**2**) are formed *in vivo*.[16,17] In contrast, there have been numerous studies examining the *in vitro* generation of 2-oxo-histidine via metal-catalysed oxidation (MCO) reactions.[17–22] These studies include the use of 2-oxo-histidine as a potential biological marker for oxidatively modified proteins,[21] selective generation of 2-oxo-histidine following exposure of the active site of Cu, Zu-superoxide dismutase to hydrogen peroxide,[22] and a study of the potential mechanisms behind metal-catalysed oxidation of histidine.[19]

A common theme in these studies is the use of tandem mass spectrometry (MS/MS) to identify and locate 2-oxo-histidine residues within peptides. Vachet and co-workers have highlighted the potential for misassignment of oxidised residues when MS/MS is carried out on protonated peptides that may contain more than one site of oxidation.[18] This is a consequence of 2-oxo-histidine formation changing the fundamental gas-phase chemistry of the histidine residue. Thus while preferential cleavage C-terminal to a histidine residue occurs to yield a b ion with a bicyclic structure,[23–26] oxidised histidine residues have been reported to suppress this cleavage.[18] It was suggested that oxidation of the histidine residues reduces the nucleophilicity of the imino nitrogen,[18] thereby preventing backbone cleavage of the peptide via a neighbouring group attack initiated by the imidazole side chain.

Apart from these studies, very little is known about the fundamental gas-phase chemistry of 2-oxo-histidine. For example, the preferred tautomeric forms of 2-oxo-histidine (**2A–2C** in Scheme 2) and protonated 2-oxo-histidine appear

**Correspondence to*: R. A. J. O'Hair, School of Chemistry, The University of Melbourne, Victoria 3010, Australia.
E-mail: rohair@unimelb.edu.au
†Part 74 of the series 'Gas-Phase Ion Chemistry of Biomolecules'.

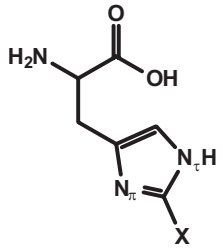


**1**: X=H
**2**: X=OH
**3**: X=SH

**Scheme 1.**

to be unknown. Here we use a combination of multistage mass spectrometry experiments and density functional theory (DFT) calculations to compare the gas-phase chemistry of protonated histidine (**1**) with that of 2-oxo-histidine (**2**), and its sulfur analogue 2-thioxo-histidine (**3**).[27]

## EXPERIMENTAL

### Chemicals

All chemicals and reagents used were of analytical grade or higher and obtained from commercial sources. With the exception of dimethylformamide (DMF) and EtOH, which were distilled before use, all chemicals were used without further purification. $CDCl_3$ (99.8 atom % deuterium) and $D_2O$ (99.9 atom % deuterium) were from Cambridge Isotope Laboratories (Andover, MA, USA). HPLC grade solvents were used for all mass spectrometry studies and obtained from Burdick & Jackson (Muskegon, MI, USA).

### Synthesis

2-Thioxo-histidine and 2-oxo-histidine were synthesised via the methods of Hegedus,[28] and Furuta and co-workers,[27] as outlined in Scheme 3. Products were characterised by their $^1$H NMR spectra, measured on an Inova-500 spectrometer (Varian, Palo Alto, CA, USA). Chemical shifts of samples in $CDCl_3$ are reported relative to the residual $CHCl_3$ peak ($\delta$ 7.26).

*Bromoacetone* (**4**)

To a solution of water (160 mL) and acetone (50 mL, 0.68 mol) was added glacial acetic acid (37.2 mL). The mixture was heated to 65°C and then bromine (35.4 mL, 0.69 mol) was added dropwise. Within 30 min after the final addition a colourless solution had resulted, which was diluted with 80 mL of cold water and cooled to 10°C. The solution was made neutral to Congo red by addition of $CaCO_3$ and the resulting organic layer that separated was dried over $CaCl_2$, then fractionally distilled, with the fraction boiling at 38–48°C/13 millibar collected to give pure **4** (25.0 mL, 44%); b.p. 38–48°C/13 millibar (lit.,[29] 40–42°C/13 millibar); $\delta_H$ (500 MHz, $CDCl_3$) 3.90 (2 H, s, $CH_2Br$), 2.37 (3 H, s, $CH_3$).

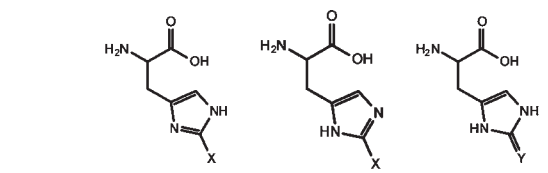


| | | | | |
|---|---|---|---|---|
| X = H | | 1A | 1B | - |
| X = OH | Y = O | 2A | 2B | 2C |
| X = SH | Y = S | 3A | 3B | 3C |

**Scheme 2.**

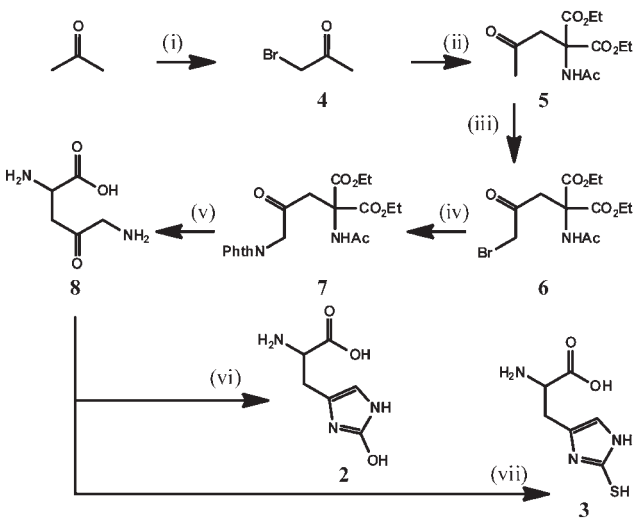


**Scheme 3.** *Reagents and conditions*: (i) $Br_2$, 65°C; (ii) diethyl acetamidomalonate, 10–15°C; (iii) $Br_2$, 40–45°C; (iv) potassium phthalimide; (v) HCl, reflux; (vi) NaOCN, 85°C; (vii) NaSCN, 85°C.

*Diethyl 2-acetamido-2-acetonylmalonate* (**5**)

Under a nitrogen atmosphere, to a solution prepared by addition of Na (0.90 g, 38.93 mmol) to anhydrous EtOH (50 mL) was added diethyl acetamidomalonate (8.06 g, 37.12 mmol). This solution was cooled to 10–15°C and **4** (3.25 mL, 38.77 mmol) added dropwise to give a gold coloured solution. Following stirring for 18 h at room temperature, the resulting NaBr was removed by filtration and the solvent evaporated to dryness *in vacuo*. The resultant yellow solid was dissolved in $CHCl_3$ and washed with water. The organic layer was dried using $Na_2SO_4$, filtered, and the solvent removed *in vacuo*. The residue was crystallised from diethyl ether to give the crude product as a white solid. Recrystallisation from EtOH gave the pure product **5** as crystals (4.50 g, 44%); m.p. 99–102°C (lit.,[27] 104–107°C); $\delta_H$ (500 MHz, $CDCl_3$) 4.23 (4 H, q, *J* 7.0 Hz, $CO_2C\underline{H}_2CH_3$), 3.73 (2 H, s, $COCH_2C$), 2.13 (3 H, s, $CH_3COC$), 2.08 (3 H, s, NHAc), 1.23 (6 H, t, *J* 7.0 Hz, $CO_2CH_2C\underline{H}_3$); *m/z* ($ES^+$) 296.2 ($[M+H]^+$, 100); HRMS ($ES^+$) Calcd. for $[C_{12},H_{19},N_1,O_6,Na]^+$ ($[M+Na]^+$) 296.11046. Found 296.11036.

*Diethyl 2-acetamido-2-(3-bromo-2-oxopropyl)malonate* (**6**)

To a solution of **5** (2.96 g, 10.81 mmol) in glacial acetic acid (9 mL) at 40–45°C was added dropwise bromine (0.54 mL, 10.54 mmol) in glacial acetic acid (3 mL). After 10–15 min the colour of the solution changed from brown to translucent yellow, whereupon the reaction mixture was cooled and concentrated *in vacuo* to give ca. 3 mL of a dark gold solution. The solution was washed with water, dried using $Na_2SO_4$ and the solvent removed to yield a light yellow solid. The crude product was crystallised from hot diisopropyl ether. Recrystallisation from EtOH gave compound **6** as colourless





DOI: 10.1002/rcm

crystals (0.99 g, 26.8%); m.p. 89–92°C (lit.,[27] 95–96°C); $\delta_H$ (500 MHz, $CDCl_3$) 4.26 (4 H, q, *J* 7.0 Hz, $CO_2C\underline{H}_2CH_3$), 3.93 (2 H, s, $BrCH_2$), 3.89 (2 H, s, $COCH_2C$), 2.02 (3 H, s, NHAc), 1.26 (6 H, t, *J* 7.0 Hz, $CO_2CH_2C\underline{H}_3$); *m/z* ($ES^+$) 352.2 ($[M+H]^+$, 100); HRMS ($ES^+$) Calcd. for $[C_{12},H_{19},N_1,O_6,Br]^+$ ($[M+H]^+$) 352.03903. Found 352.03806.

*Diethyl 2-acetamido-2-(2-oxo-3-phthalimidopropyl) malonate* (**7**)

Under a nitrogen atmosphere, to a solution of **6** (8.31 g, 23.59 mmol) in anhydrous DMF (3 mL) was added potassium phthalimide (4.81 g, 25.95 mmol). The resulting brownish red mixture was stirred at 50°C for 90 min, cooled and extracted into $CHCl_3$. The extract was washed successively with brine (10 mL), 3% NaOH (10 mL), 3% HCl (10 mL) and brine (2 × 10 mL). The organic layer was concentrated *in vacuo* to give a dark yellow solution which crystallised upon standing for ca. 1 h. Recrystallisation from diethyl ether gave **7** as a creamy white solid (7.79 g, 79%); m.p. 168-170°C (lit.,[27] 170–171°C); $\delta_H$ (500 MHz, $CDCl_3$) 7.86–7.73 (4 H, m, $C_6H_4$), 4.46 (2 H, s, $NCH_2$), 4.24 (4 H, q, *J* 7.0, Hz, $CO_2C\underline{H}_2CH_3$), 3.82 (2 H, s, $COCH_2C$), 2.06 (3 H, s, NHAc), 1.24 (6 H, t, *J* 7.0 Hz, $CO_2CH_2C\underline{H}_3$); *m/z* ($ES^+$) 419.3 ($[M+H]^+$, 100); HRMS ($ES^+$) Calcd. for $[C_{20},H_{23},N_2,O_8]^+$ ($[M+H]^+$) 419.14489. Found 419.14482.

*DL-2,5-Diamino-4-oxopentanoic acid dihydrochloride* (**8**)

A suspension of **7** (6.49 g, 15.52 mmol) in 37% HCl (20 mL) was heated at reflux for 6 h. The reaction mixture was cooled to room temperature and allowed to stand overnight at 4°C. The precipitated phthalic acid was removed by filtration and the mixture concentrated *in vacuo*. Concentrated HCl (5 mL) was added to the residue and the solution filtered to yield a dark tan solution. This solution was treated twice with activated charcoal, to yield a light brown solution. The solution was heated at 50°C for 1 h to afford an olive green solution, which was filtered through activated carbon and Celite. EtOH (100 mL) was added and the yellow solution was allowed to stand overnight at 4°C to give compound **8** as white crystals (1.65g, 49%); *m/z* ($ES^+$) 147.1 ($[M+H]^+$, 100); HRMS ($ES^+$) Calcd. for $[C_5,H_{11},N_2,O_3]^+$ ($[M+H]^+$) 147.07642. Found 147.07646.

*DL-2-Oxo-histidine* (**2**)

To a solution of **8** (0.52 g, 2.36 mmol) in water (400 μL) at 95°C was added potassium cyanate (0.39 g, 4.76 mmol). The reaction mixture was heated at 85°C with stirring for 1 h. Saturated aqueous NaOAc (12 mL) was added and the mixture was allowed to stand for 24 h at 0°C to give crude **2** as a creamy white solid (0.16 g, 40%); $\delta_H$ (500 MHz, $D_2O$) 6.39 (1H, s, ArH), 3.88 (1 H, dd, *J* 8.5, 5.0 Hz, $C\underline{H}NH_2$), 3.07 (1H, ddd, J 16.0, 4.5, 0.5 Hz, $C\underline{H}HCHNH_2$), 2.93 (1H, dd, *J* 15.5, 8.0 Hz, $CH\underline{H}CHNH_2$); *m/z* ($ES^+$) 172.1 ($[M+H]^+$); HRMS ($ES^+$) Calcd. for $[C_6,H_{10},N_3,O_3]^+$ ($[M+H]^+$) 172.07167. Found 172.07166.

*DL-2-Thioxo-histidine* (**3**)

To a solution of **8** (0.52 g, 2.35 mmol) in water (500 μL) at 95°C was added potassium thiocyanate (0.49 g, 6.06 mmol). The reaction mixture was heated at 85°C with stirring for 1 h. Saturated aqueous NaOAc (5 mL) was added and the mixture was allowed to stand for 24 h at 0°C. The solid was collected by filtration and washed with water and ethanol to give crude **3** (0.07 g, 17%); $\delta_H$ (500 MHz, $D_2O$) 6.88 (1H, s, ArH), 3.96 (1H, dd, *J* 8.5, 5.0 Hz, $C\underline{H}NH_2$), 3.22 (1H, ddd, *J* 15.5, 5.0, 0.5 Hz, $C\underline{H}HCHNH_2$), 3.10 (1H, dd, *J* 16.5, 8.5 Hz, $CH\underline{H}CHNH_2$); *m/z* ($ES^+$) 188.1 ($[M+H]^+$); HRMS ($ES^+$) Calcd. for $[C_6,H_{10},N_3,O_2,S]^+$ ($[M+H]^+$) 188.04882. Found 188.04876.

## C-terminal methylation of the histidine derivatives

The histidine derivative (10 mg) was dissolved in 1 mL of a solution prepared by dropwise addition of acetyl chloride (800 μL) to anhydrous methanol (5 mL), and the mixture was allowed to stand for 2 h at room temperature. The samples were lyophilised and used without purification.

## Mass spectrometry

Multistage mass spectrometry experiments were carried out using a commercially available hybrid linear ion trap and Fourier transform ion cyclotron resonance (FT-ICR) mass spectrometer (Finnigan LTQ-FT; Thermo Scientific, Bremen, Germany), equipped with an electrospray ionisation (ESI) source. Samples were prepared by dissolving approximately 0.1 mg of the analyte in 140 μL of MeOH; a 10 μL aliquot of this stock solution was diluted with 140 μL of MeOH. This solution was introduced into the mass spectrometer via direct injection into the ESI source at a flow rate of 5 μL/min. The sheath gas flow rate, capillary voltage, and temperature were adjusted to ca. 3–25 (arbitrary units), 3.0–8.0 kV, and 275°C, respectively. Collision-induced dissociation (CID) experiments were performed within the LTQ using standard procedures of mass-selecting the desired precursor ion, usually with an isolation width of 1.5 *m/z* units, and subjecting the ion to CID conditions with an activation Q value of 0.25 for a period of 30 ms and a normalised collision energy which ensures that the intensity of the precursor ion is approximately 10–20% of intensity of the base peak.

High-resolution mass spectrometry (HRMS) data were obtained by transferring ions of interest from the linear ion trap into the FT-ICR cell. Positive mode calibration was performed via the in-built automatic calibration function using the recommended LTQ-FT calibration solution, consisting of caffeine, the short tetrapeptide MRFA, and Ultramark 1621.

## Theoretical methods

Quantum chemical calculations were performed using the Gaussian 03 molecular modelling package[30] using the hybrid DFT B3-LYP[31,32] model in conjunction with the standard 6-311++G(d,p) basis set. A thorough examination of the complete conformational space of both 2-oxo-histidine and 2-thioxo-histidine is beyond the scope of this study. Instead, a range of possible conformers for each system was constructed through rotation of the major dihedrals in 90° increments. These structures were optimised at the B3-LYP/6-31G(d) level of theory, with the lowest energy structures for each tautomer being reoptimised at the B3-LYP/6-311++G(d,p) level. All optimised structures were subjected to vibrational frequency analysis to ensure that they corresponded to either a local minimum (no imaginary frequencies) or a transition state (one imaginary frequency). Intrinsic reaction coordi-





DOI: 10.1002/rcm

nate[33] (IRC) calculations followed by geometry optimisations were performed on each transition state to ensure that the reaction path originating from the transition state was connected to the appropriate reactant and product minima. The final energies used to calculate the potential energy surfaces were corrected with the zero-point vibrational energies obtained from the frequency calculations. No scaling factors were utilised. In order to account for entropy and temperature effects, unless noted otherwise, all energy values refer to the Gibbs free energy values at 298.15 K ($\Delta G_{298}$).

The proton affinities (PAs) and gas-phase basicities (GBs) of the three histidine species were calculated via the following equations:

$$M + H^+ \rightarrow [M + H]^+$$

$$-PA = \Delta_r H_{298} = E_{electronic_+ Thermal\ Enthalpies}([M + H]^+) - E_{electronic_+ Thermal\ Enthalpies}(M) - 5/2RT$$

$$-GB = \Delta_r G_{298} = E_{electronic_+ Thermal\ Free\ Energies}([M + H]^+) - E_{electronic_+ Thermal\ Free\ Energies}(M) - 5/2RT + E_{vibrational}([M + H]^+) - E_{vibrational}(M) - S(H^+).^{34}$$

## RESULTS AND DISCUSSION

We first describe results of DFT calculations aimed at examining the tautomers of neutral and protonated amino acids **1**, **2** and **3**. Experiments that provide relative proton affinity orders of **1**, **2** and **3** are then outlined, followed by an estimation of their proton affinities and gas-phase basicities via DFT calculations. The CID spectra of protonated **1**, **2** and **3** and their methyl esters are presented, followed by DFT calculations aimed at examining the potential energy surfaces (PES) giving rise to the observed product ions.

### DFT calculations on the neutral tautomers of 2-oxo-histidine, 2-thioxo-histidine and histidine

Using DFT calculations, we have examined the most stable conformations of each of the three tautomers **A**, **B** and **C** (Scheme 2) of 2-oxo-histidine, **2**, and 2-thioxo-histidine, **3**, as well as both tautomers **A** and **B** for histidine, **1**, which have been adapted from a previous study.[35] The results of these calculations are summarised in Table 1, which shows the structure of the most stable conformation of each tautomer, as well as its energy expressed relative to the specific histidine derivative global minima (shown in italics in kcal.mol$^{-1}$). An examination of Table 1 reveals that tautomer **B**, where the hydrogen atom in located on $N_\pi$, is always slightly more stable than tautomer **A**, in which the hydrogen atom is on $N_\tau$ (0.2–0.8 kcal.mol$^{-1}$), which is consistent with the work by Kovačević and coworkers.[35] This may be due to the different hydrogen-bonding arrangements for these tautomers: **A** forms a seven-membered ring between the hydroxy group and basic side-chain $N_\pi$, while **B** involves formation of five- and seven-membered rings involving the amino and hydroxy groups and the carbonyl carbon and basic side-chain N, respectively.

**Table 1.** Lowest energy tautomers of neutral histidine, 2-oxo-histidine and 2-thioxo-histidine. All energies are listed as relative $\Delta G_{298}$ to their most stable neutral conformer, **1A**, **2C** and **3C** (in kcal.mol$^{-1}$), with the structures optimised at the B3-LYP/6-311++G(d,p) level

| | Tautomer | | |
|---|---|---|---|
| | 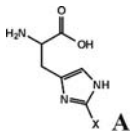 **A** | 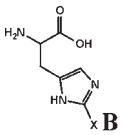 **B** | 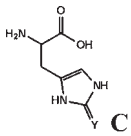 **C** |
| histidine (X = H) | 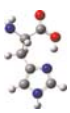 **1A** *0.2* | 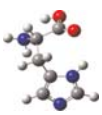 **1B** *0.0* | — |
| 2-oxo-histidine (X = OH, Y= O) | 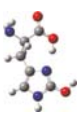 **2A** *8.2* | 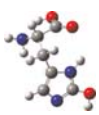 **2B** *7.4* | 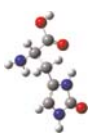 **2C** *0.0* |
| 2-thioxo-histidine (X = SH, Y = S) |  **3A** *4.4* | 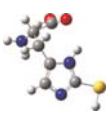 **3B** *4.1* |  **3C** *0.0* |





DOI: 10.1002/rcm

Due to the presence of the hydroxyl and thiol groups, 2-oxo-histidine and 2-thioxo-histidine are able to adopt the '**C**' oxo/thioxo tautomers. In each case, this tautomer is more stable than both **A** and **B**. This observation that the keto/thioketo tautomer is favoured over the enol/thioenol tautomer is consistent with previous studies on related imidazolones. Thus X-ray crystallography studies[36,37] and theoretical calculations[38] both show a preference for the keto/thioketo tautomer.

## DFT calculations on the protonated tautomers of 2-oxo-histidine, 2-thioxo-histidine and histidine

There is a variety of potential protonation sites for each histidine tautomer: (i) the amino nitrogen ($\mathbf{N_{Amino}}$); (ii) one of the two side-chain nitrogen atoms, $N_\pi$ or $N_\tau$, ($\mathbf{N_{Sidechain}}$); (iii) the carbonyl oxygen ($\mathbf{O_{Carbonyl}}$); and in the case of 2-oxo-histidine (**2**) and 2-thioxo-histidine (**3**), (iv) the side-chain *O*- or *S*-heteroatom ($\mathbf{O_{Sidechain}}$) (Scheme 4). Of the nine potential structures for **2** and **3**, three of these structures are identical, $\mathbf{AN_{Sidechain}}$, $\mathbf{BN_{Sidechain}}$ and $\mathbf{CO_{Sidechain}}$, leading to a total of seven unique structures. As tautomer **C** does not exist for histidine, only five structures were examined for protonated histidine. A comparison of the relative energies for each of these structures can be found in Table 2.

From the structures shown in Table 2 it appears that for each 'type' of protonated structure, e.g. $\mathbf{AN_{Sidechain}}$, a common conformation is adopted for all three histidines, in a similar manner to the neutral conformers in Table 1. The energies of these various structures appear to be dictated by the extent of stabilisation of the ionising proton. The charge of the ionising proton for the lowest-energy structures of all three histidine species, $\mathbf{AN_{Sidechain}}$, is delocalised over the imidazole side chain. These structures also exhibit extensive hydrogen bonding, with the ionising proton stabilised by a six-membered ring involving the amino group, of which one of its hydrogen atoms is further stabilised by a distorted five-membered ring involving the carbonyl oxygen.

From Table 2 some general trends can be observed regarding the preferred protonatation sites: (i) due to the potential for resonance stabilisation, the preferred site of protonation is on the side-chain; (ii) protonation on the amino moiety is only favoured when the ionising proton can be stabilised by hydrogen bonding, as in the case of $\mathbf{AN_{Amino}}$; and (iii) due to the lack of stabilisation, protonation on the carbonyl oxygen to yield a diol is unfavourable, leading to the high-energy structures $\mathbf{AO_{Carbonyl}}$, $\mathbf{BO_{Carbonyl}}$ and $\mathbf{CO_{Carbonyl}}$. Finally, in contrast to the neutral tautomers, where the difference in energy between each structure was similar for all three histidine systems, protonation results in a greater variation of the energies.

## Proton affinities and gas-phase basicities of histidine, 2-oxo-histidine and 2-thioxo-histidine

As the relative proton affinities (PAs) of amino acid residues in a peptide form the basis of the 'mobile proton' fragmentation model, post-translational modification of amino acids that alter the proton affinity of a residue can influence the fragmentation reactions observed. A key example of this is the increase in proton affinity following oxidation of methonine residues,[39] resulting in the preferential loss of $CH_3SOH$.[11,13] In contrast, oxidation of the side chain of histidine was proposed to reduce the nucleophilicity of the imidazole ring, thus suppressing cleavage C-terminal to the modified histidine residue.[18] As this reduction in nucleophilicity would be expected to be reflected in a reduction in the PA of 2-oxo-histidine, a focus of this work was to investigate how modification of the histidine side chain can affect the proton affinity.

Although a quantitative experimental examination of the proton affinities of both 2-oxo-histidine and 2-thioxo-histidine using Cooks' kinetic method[40,41] or the extended

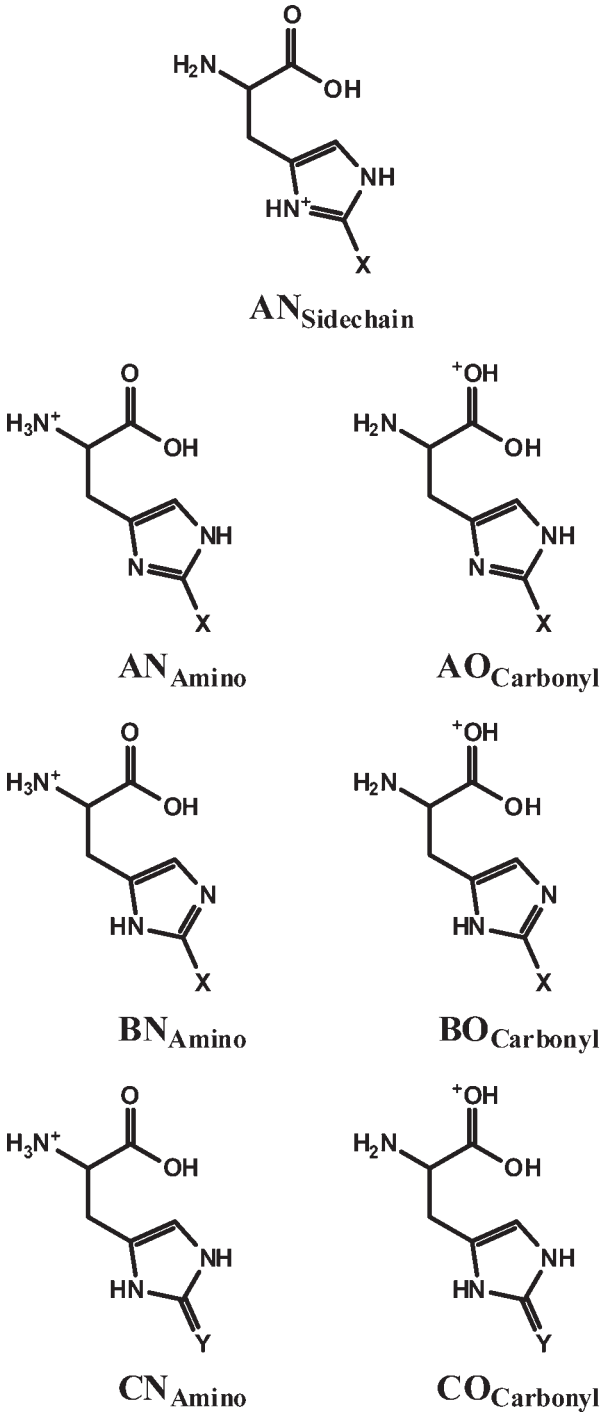


**Scheme 4.**





DOI: 10.1002/rcm

**Table 2.** Lowest energy tautomers of protonated histidine, 2-oxo-histidine and 2-thioxo-histidine. All energies are listed as relative $\Delta G_{298}$ to their most stable protonated conformer, **H09a**, **09a** and **M09a** (in kcal.mol$^{-1}$), with the structures optimised at the B3-LYP/6-311++G(d,p) level

| | Protonated Structure | | | | | | |
|---|---|---|---|---|---|---|---|
| | $AN_{Sidechain}$ | $AN_{Amino}$ | $AO_{Carbonyl}$ | $BN_{Amino}$ | $BN_{Carbonyl}$ | $CN_{Amino}$ | $CO_{Carbonyl}$ |
| histidine (X = H) | 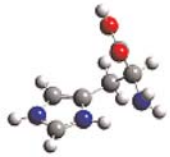 **$1AN_{Sidechain}$/H9a** *0.0* | 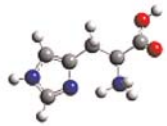 **$1AN_{Amino}$** *1.8* | 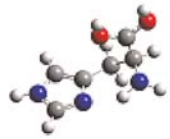 **$1AO_{Carbonyl}$** *42.9* | 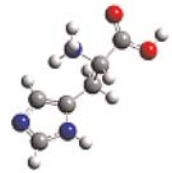 **$1BN_{Amino}$** *20.8* | 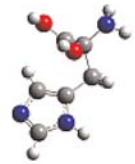 **$1BN_{Carbonyl}$** *51.1* | – | – |
| 2-oxo-histidine (X = OH, Y = O) | 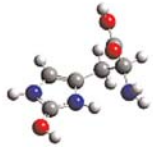 **$2AN_{Sidechain}$/10a** *0.0* | 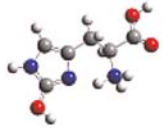 **$2AN_{Amino}$** *0.5* |  **$2AO_{Carbonyl}$** *40.4* | 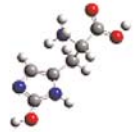 **$2BN_{Amino}$** *15.3* | 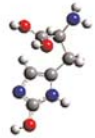 **$2BN_{Carbonyl}$** *46.0* | 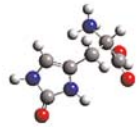 **$2CN_{Amino}$** *10.9* | 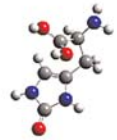 **$2CO_{Carbonyl}$** *37.9* |
| 2-thioxo-histidine (X = SH, Y = O) | 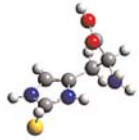 **$3AN_{Sidechain}$/M11a** *0.0* | 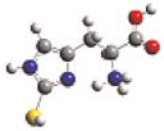 **$3AN_{Amino}$** *2.1* | 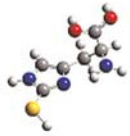 **$3AO_{Carbonyl}$** *42.5* | 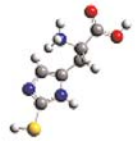 **$3BN_{Amino}$** *19.2* | 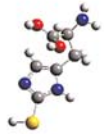 **$3BN_{Carbonyl}$** *49.5* | 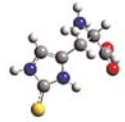 **$3CN_{Amino}$** *19.4* | 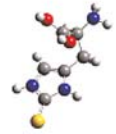 **$3CO_{Carbonyl}$** *45.3* |





DOI: 10.1002/rcm

kinetic method[42,43] via the use of reference bases is beyond the scope of this work, the proton affinities of histidine, 2-oxo-histidine and 2-thioxo-histidine were obtained via CID of proton-bound heterodimers. In order to validate these experimental results and to gain estimates of these intrinsic chemical properties of 2-oxo-histidine and 2-thioxo-histidine, DFT calculations on the neutral and protonated tautomers, shown in Table 1 and 2, were used to calculate the proton affinities and gas-phase basicities for all the possible protonation sites of the various tautomers.

## Relative proton affinities of histidine, 2-oxo-histidine and 2-thioxo-histidine via competitive dissociation of proton-bound dimers

The proton affinity order of histidine, 2-oxo-histidine and 2-thioxo-histidine was determined experimentally through the kinetic method developed by Cooks.[40,41] This involves the competitive dissociation of a proton-bound dimer, which upon low-energy CID dissociates into its respective protonated monomers, with the relative abundance of the two ions being dependent on the relative proton affinities of the two neutral monomers.

The CID spectra of all the three possible combinations of proton-bound heterodimers were measured: (i) [histidine–$H^+$–2-oxo-histidine]$^+$; (ii) [histidine–$H^+$–2-thioxo-histidine]$^+$; and (iii) [2-oxo-histidine–$H^+$–2-thioxo-histidine]$^+$. The low-energy CID of the dimer (i) is shown in Fig. 1(A), with the spectrum dominated by the ion at $m/z$ 156 corresponding to protonated histidine, indicating that histidine has a greater PA than 2-oxo-histidine. Likewise the PA of histidine is greater than that of 2-thioxo-histidine (Fig. 1(B)). Finally, 2-thioxo-histidine has a greater PA than 2-oxo-histidine (Fig. 1(C)). From these results, we can determine that the proton affinity order is: PA(histidine) > PA (2-thioxo-histidine) > PA (2-oxo-histidine). The gas-phase basicity order is expected to follow the same trend as the differences in entropy between the three histidines are expected to be minimal owing to the common conformations that are adopted for the neutral and protonated tautomers.

## DFT estimates of the local proton affinities and gas-phase basicities of histidine, 2-oxo-histidine and 2-thioxo-histidine

Using Tables 1 and 2, the proton affinities ('local proton affinities') and gas-phase basicities ('local gas-phase basicities') at each protonation site for each of the tautomers of histidine, 2-oxo-histidine and 2-thioxo-histidine were determined. Scheme 5 shows both the proton affinity and gas-phase basicity (in kcal.mol$^{-1}$) for each protonation site, denoted by the number next to it, with the highest value for each structure underlined. In addition, the relative free energies of each structure (in kcal.mol$^{-1}$) are shown and are expressed relative to the specific histidine global minima (shown below the conformer label).

From Scheme 5 a number of observations can be made on the gas-phase basicities and the related proton affinities of the three histidines:

i. The values for each protonation site reflect the relative stabilities of the final protonated products. More stable protonated products mean a higher local proton affinity;

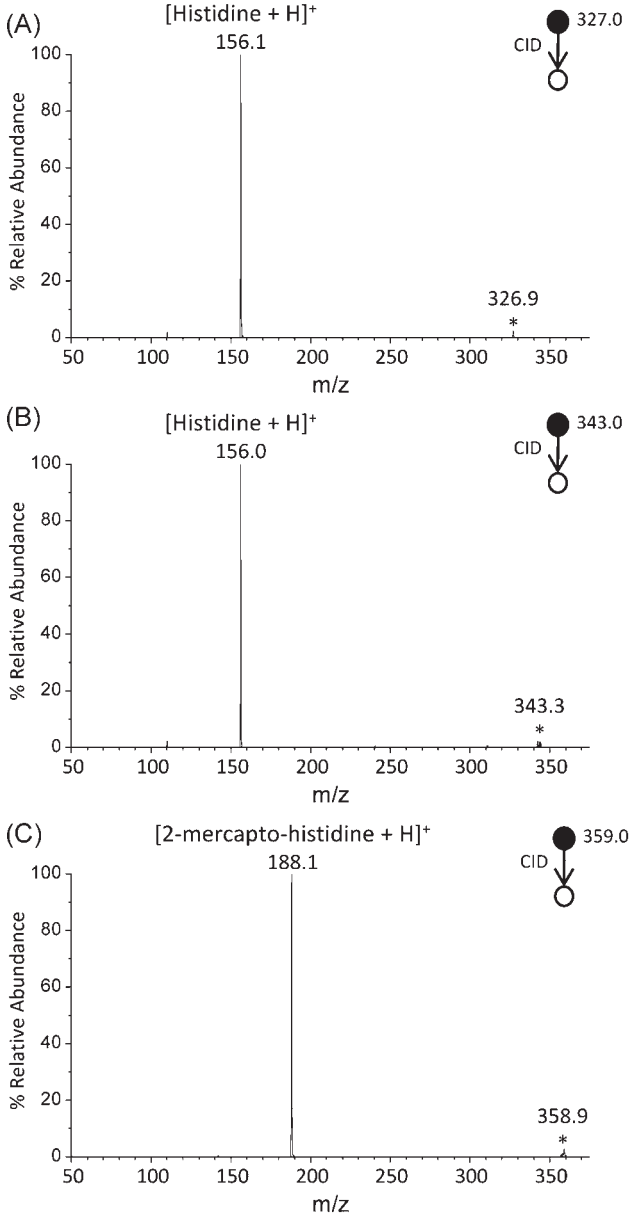


**Figure 1.** LTQ collision-induced dissociation MS/MS spectra of proton-bound dimers: (A) [histidine–$H^+$–2-oxo-histidine]$^+$; (B) [histidine–$H^+$–2-thioxo-histidine]$^+$; and (C) [2-oxo-histidine–$H^+$–2-thioxo-histidine]$^+$. An asterisk refers to the mass-selected precursor ion.

ii. The calculated gas-phase basicity for histidine of 221.4 kcal.mol$^{-1}$ is comparable with the experimental values of 223.7 and 227.1 kcal.mol$^{-1}$ reported by Harrison and co-workers,[46] and Hunter and Lias,[47] respectively. However, our proton affinity value of 227.4 kcal.mol$^{-1}$ differs from the computed values of 233.9 (G3MP2) and 236.4 (B3LYP/6-311+G(d,p)) kcal.mol$^{-1}$ by Gronert *et al.*[44] and Leszczynski and coworkers.[45]

iii. The gas-phase basicities for the lowest-energy neutral structures of 2-oxo-histidine (**2C**) and 2-thioxo-histidine (**3C**) are 210.7 and 218.4 kcal.mol$^{-1}$, respectively, indicating that the simple addition of an oxygen or sulfur atom onto the imidazole ring lowers the gas-phase basicity.





DOI: 10.1002/rcm

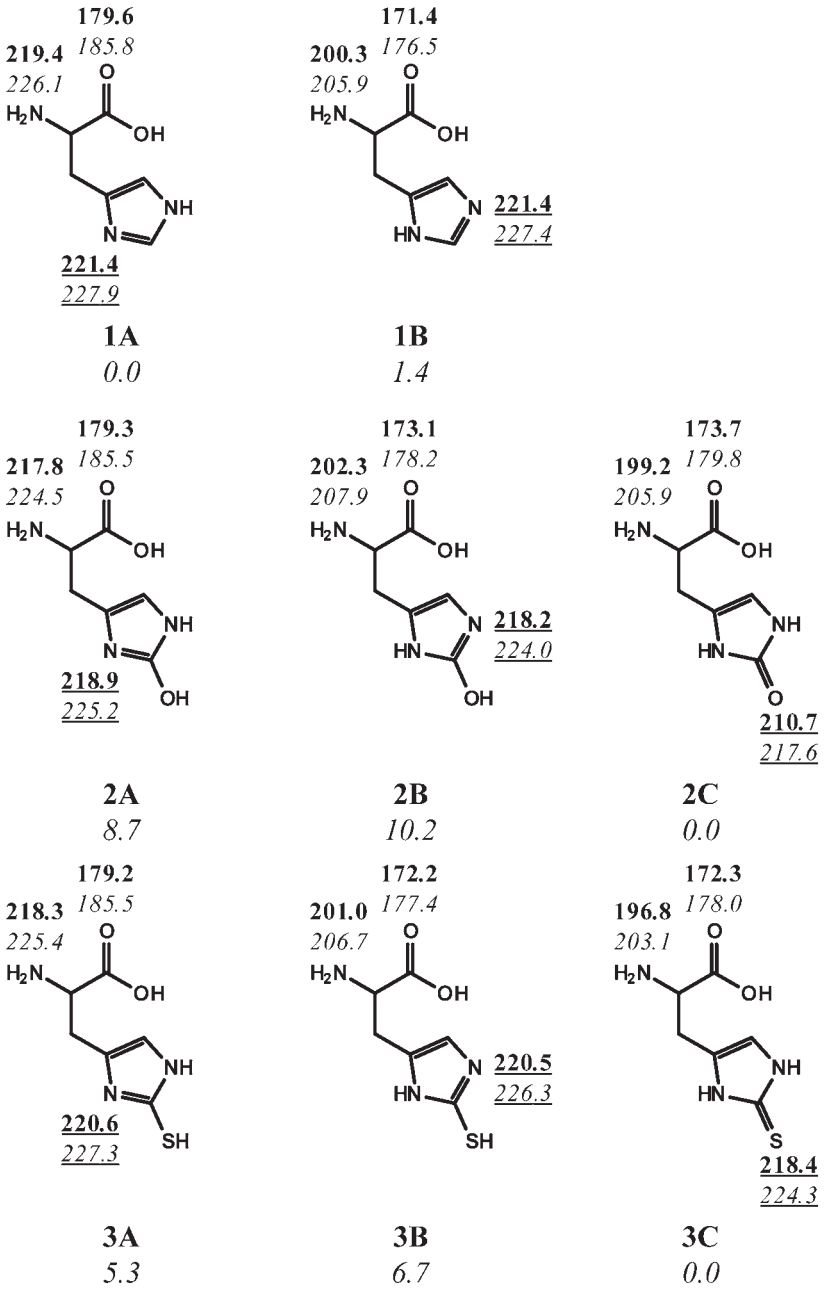


**Scheme 5.** Local proton affinities and gas-phase basicities of the various tautomers of protonated: histidine, 2-oxo-histidine and 2-thioxo-histidine. Each possible protonation site is labelled with an energy value (in kcal.mol$^{-1}$) denoting its gas-phase basicity (in bold) and proton affinity (in italics) at 298 K, with the structures optimised at the B3-LYP/6-311++G(d,p) level. Values that are underlined denote the local site with the highest proton affinity and gas-phase basicity, while the values listed below each structure correspond to the lowest energy tautomers of each histidine derivative and are listed as relative $\Delta G_{298}$ to their most stable neutral conformer, **1A**, **2C** and **3C** (in kcal.mol$^{-1}$).

These values are in agreement with the proton affinity order obtained experimentally;

iv. Interestingly, the gas-phase basicities and proton affinities of tautomers **A** and **B** for all three histidine systems are quite similar, indicating that the reduced proton affinity exhibited by 2-oxo-histidine and 2-thioxo-histidine is a consequence of their ability to adopt the lower energy tautomer **C**;

v. Histidine has the highest proton affinity/gas-phase basicity for all the possible protonation sites of tautomer **A**, followed by 2-thioxo-histidine and 2-oxo-histidine. The same relative trend can be observed for the ring nitrogens



DOI: 10.1002/rcm

of tautomer **B**; however, the amino nitrogen and the carbonyl oxygen show a reversal in this trend, with 2-oxo-histidine, then 2-thioxo-histidine, exhibiting higher local proton-affinities/gas-phase basicities.

## Gas-phase fragmentation chemistry of protonated 2-oxo-histidine, 2-thioxo-histidine and their derivatives

The CID spectra of protonated histidine, 2-oxo-histidine and 2-thioxo-histidine are shown in Fig. 2. All three spectra are dominated by the combined losses of $H_2O$ and CO (Eqn. (1)) to give the $a_1$ ions at $m/z$ 110 (Fig. 2(A)), 126 (Fig. 2(B)), and 142 (Fig. 2(C)). Other common reaction channels include formation of the bicyclic $b_1$ ion[23–26] (Eqn. (2)) as a minor product in each case and a minor combined loss of $CO_2$ and $NH_3$ (Eqn. (3)). A closer examination of the spectra reveals that protonated 2-oxo-histidine and 2-thioxo-histidine undergo two additional fragmentation reactions that are not observed for protonated histidine: (i) minor losses of 73 Da to yield $m/z$ 99 and 115, and (ii) the loss of $NH_3$ (Eqn. (4)) to yield $m/z$ 155 and 171 for 2-oxo- and 2-thioxo-histidine, respectively. Accurate mass measurements indicate that the ions at $m/z$ 99 and 115 are the result of the loss of $[C_2,H_3,O_2,N]$ from their respective precursor ions. This may occur via one of three possible pathways: (i) loss of HCN from the $a_1$ ion (Eqn. (5)); (ii) loss of the combined elements $CO_2$ and $[C,H_3,N]$ (Eqn. (6)); and (iii) loss of the imine $HN{=}CHCO_2H$ (Eqn. (7)). Although the signal intensities of the ions at $m/z$ 99 and 115 for 2-oxo-histidine and 2-thioxo-histidine, respectively, were too low to gain structural information from subsequent $MS^3$ studies, in order to determine whether the first mechanism can operate, the collisional activation of the $a_1$ ions of the three histidine species was performed (Figs. 2(D)–2(F)). The virtual absence of the ion at $m/z$ 115 for 2-thioxo-histidine (Fig. 2(F)) and the low abundance of the ion at $m/z$ 99 for 2-oxo-histidine (Fig. 2(E)) indicate that loss of HCN from the $a_1$ ion (Eqn. (5)) is not favoured and that this mechanism is unlikely to be

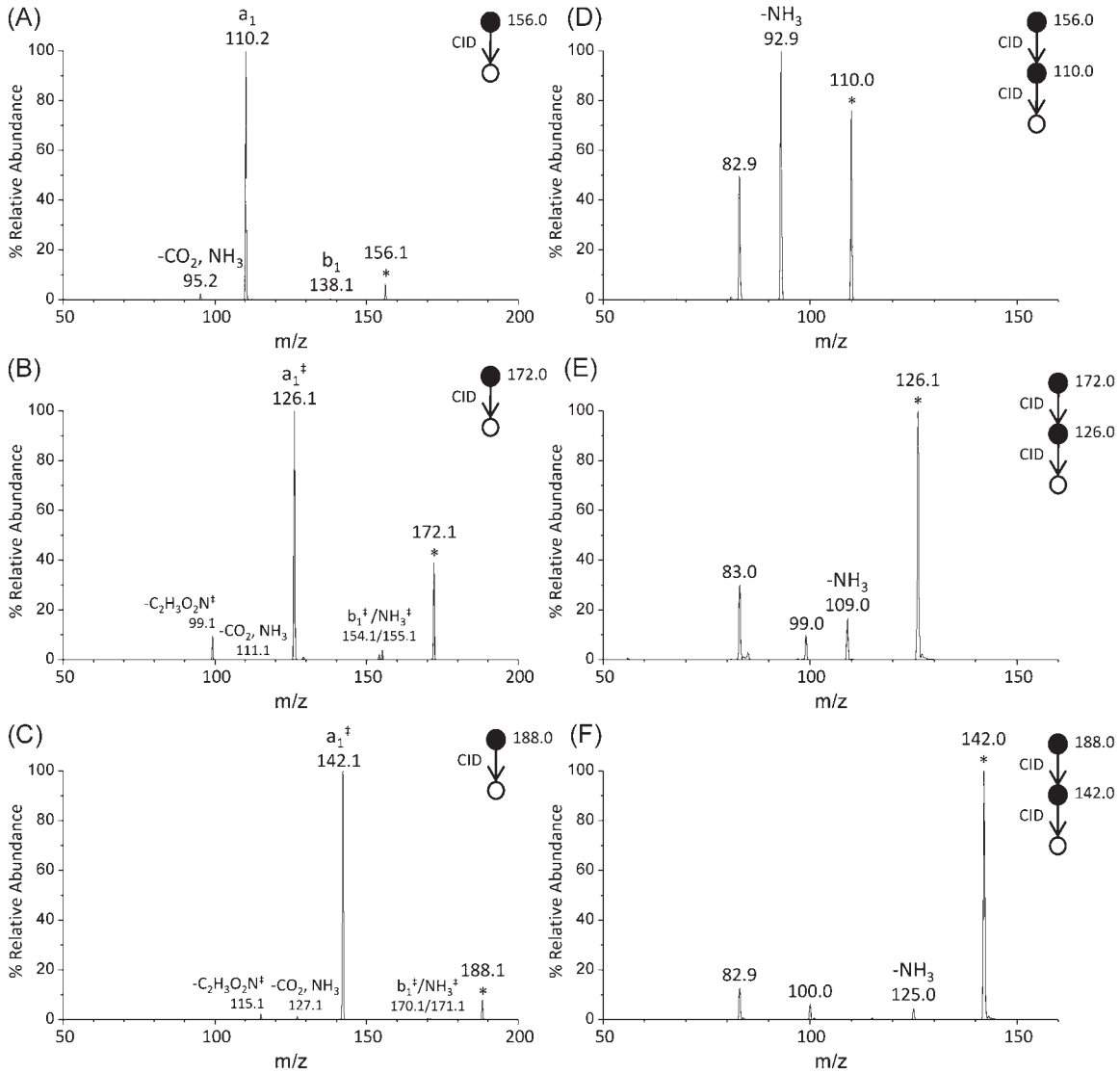


**Figure 2.** LTQ collision-induced dissociation MS/MS spectra of protonated histidine derivatives: (A) histidine; (B) 2-oxo-histidine; and (C) 2-thioxo-histidine. $MS^3$ spectra of the $a_1$ ion of protonated: (D) histidine; (E) 2-oxo-histidine; and (F) 2-thioxo-histidine. An asterisk refers to the mass-selected precursor ion. The ‡ symbol indicates that the assignment of the molecular formula of the neutral(s) lost has been confirmed via HRMS.





DOI: 10.1002/rcm

RCM

important. The potential mechanism by which $[C_5,H_5,O_2,N]$ is lost was narrowed down by MS/MS studies of the methyl ester derivatives, as described below.

$$[M+H]^+ \rightarrow [M+H-H_2O-CO]^+ + H_2O,\ CO \quad (1)$$

$$\rightarrow [M+H-H_2O]^+ + H_2O \quad (2)$$

$$\rightarrow [M+H-CO_2-NH_3]^+ + CO_2,\ NH_3 \quad (3)$$

$$\rightarrow [M+H-NH_3]^+ + NH_3 \quad (4)$$

$$\rightarrow [M+H-H_2O-CO-HCN]^+ + H_2O,\ CO,\ HCN \quad (5)$$

$$\rightarrow [M+H-CO_2-[C,H_3,N]]^+ + CO_2 + [C,H_3,N] \quad (6)$$

$$\rightarrow [M+H-HN=CHCO_2H]^+ + HN=CHCO_2H \quad (7)$$

The methyl esters of protonated 2-oxo-histidine and 2-thioxo-histidine were also investigated (Figs. 3 (B) and 3(C)). In contrast to the previously studied protonated histidine methyl ester (Fig. 3(A)) which exhibits an almost identical spectrum to protonated histidine (Fig. 2(A)),[24] introduction of a C-terminal methyl ester functionality onto 2-oxo- and 2-thioxo-histidine appears to promote minor pathways that were previously observed for the parent amino acids. This is most noticeable for protonated 2-oxo-histidine methyl ester (Fig. 3(B)), in which the $a_1$ ion at $m/z$ 126 is now disfavoured and is no longer the most abundant product ion. Instead the previously minor ion at $m/z$ 99 (Fig. 2(B)) is now the most abundant. The presence of this ion indicates that this ion is not formed via the combined loss of $CO_2$ and $[C,H_3,N]$ (Eqn. (6)), as this channel would be expected to 'switch off' for the methyl ester derivatives. Instead, this ion is proposed to arise via loss of the imine $HN{=}CHCO_2R$ (R=H or $CH_3$) (Scheme 6, Eqn. (7)). In addition, the loss of $NH_3$ to yield the ion at $m/z$ 169 is now more favoured.

Conversion of the free acid into the ester also influences the low-energy CID behaviour of protonated 2-thioxo-histidine. There is a minor increase in abundance of the $m/z$ 115 ion (Eqn. (6)), though the $a_1$ ion remains the most abundant. However, the loss of $H_2O$, CO ($m/z$ 156) was observed. This loss is presumed to occur via a retro-Koch mechanism as previously proposed by Reid *et al.*[48]

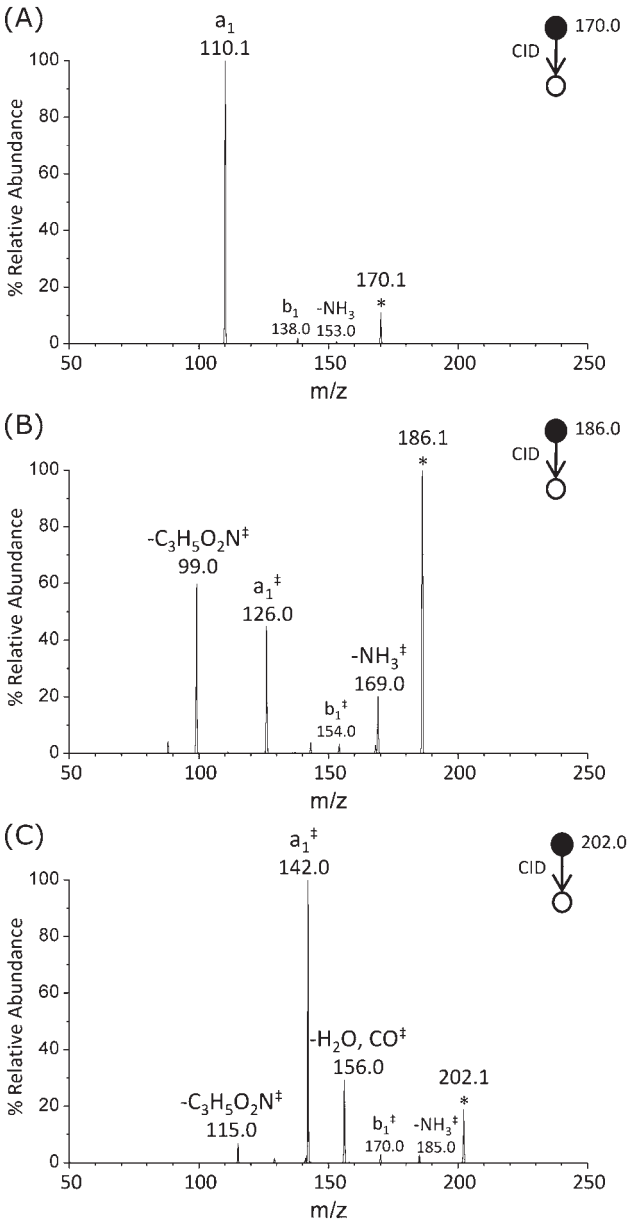


**Figure 3.** LTQ collision-induced dissociation MS/MS spectra of protonated histidine methyl ester derivatives: (A) histidine methyl ester; (B) 2-oxo-histidine methyl ester; and (C) 2-thioxo-histidine methyl ester. An asterisk refers to the mass-selected precursor ion. The ‡ symbol indicates that the assignment of the molecular formula of the neutral(s) lost has been confirmed via HRMS.

## Fragmentation mechanisms of protonated 2-oxo-histidine, 2-thioxo-histidine and histidine

To gain insight into the role that side-chain modification has on the barriers against the $H_2O$ and CO, $NH{=}CHCO_2H$ and $NH_3$ fragmentation pathways for protonated histidine, DFT calculations were used to investigate the potential energy surfaces (PES) associated with the losses of $H_2O$, CO (Eqn. (1)); $H_2O$ (Eqn. (2)); $HN{=}CHCO_2H$ (Eqn. (7)); and $NH_3$ (Eqn. (4)) from protonated 2-oxo-histidine, 2-thioxo-histidine and histidine. The PES are illustrated for 2-oxo-histidine in Figs. 4–6, while those for 2-thioxo-histidine and histidine are given in the Supporting Information.

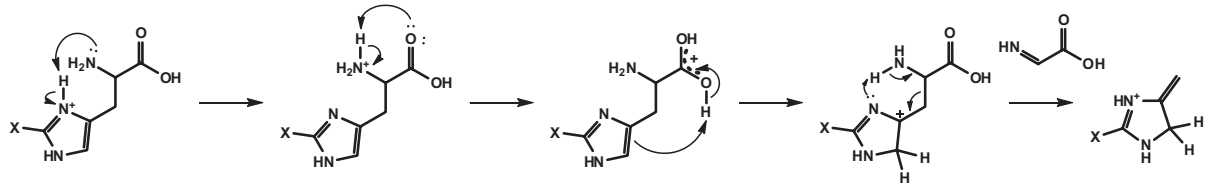

**Scheme 6.**





DOI: 10.1002/rcm

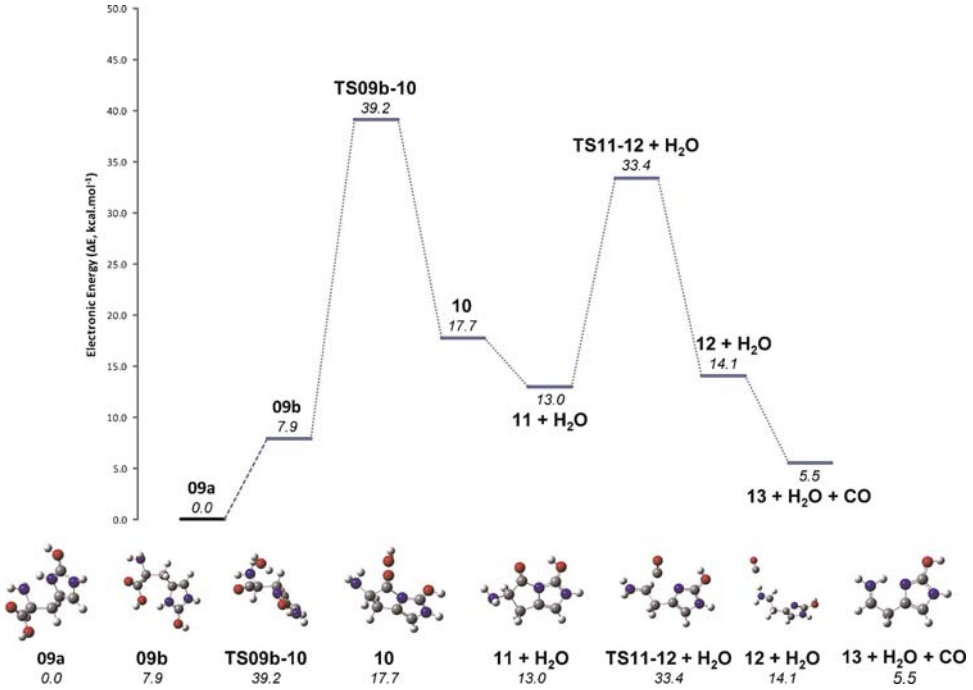


**Figure 4.** Calculated reaction pathways and key structures involved in the loss of (a) $H_2O$ and (b) $H_2O$, CO from protonated 2-oxo-histidine. All energies are listed as relative $\Delta G_{298}$ to **09a** (in kcal.mol$^{-1}$), with the structures optimised at the B3-LYP/6-311++G(d,p) level.

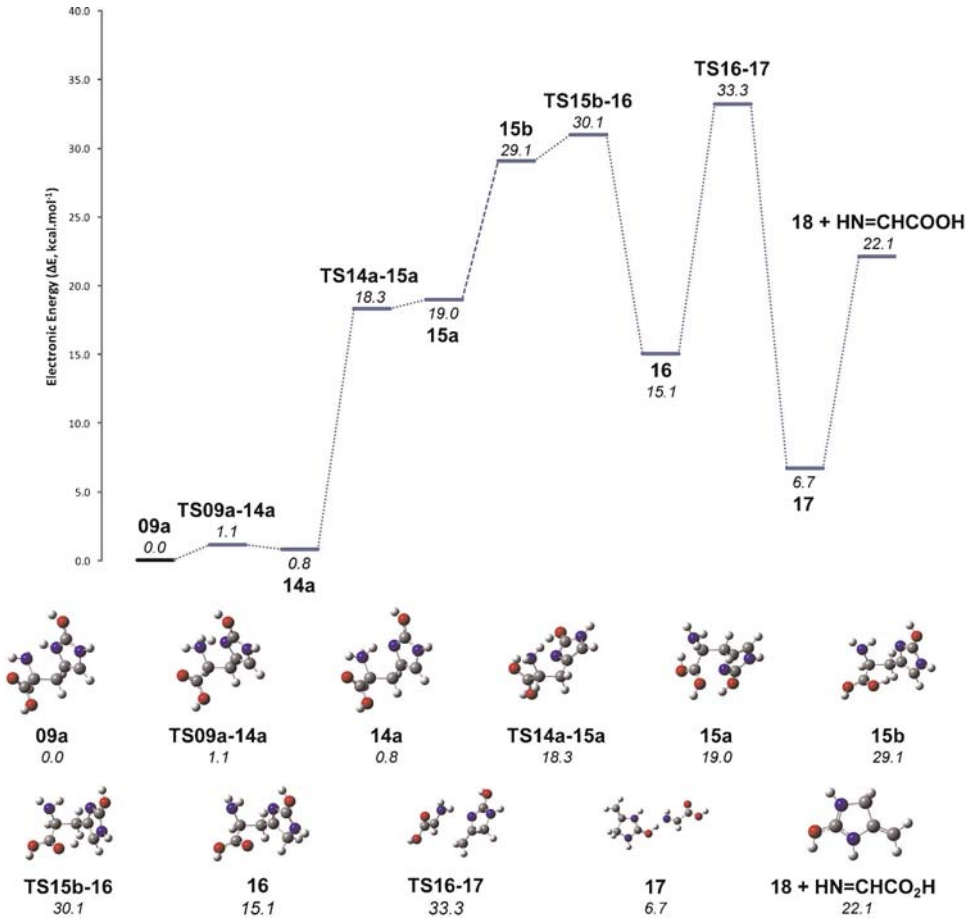


**Figure 5.** Calculated reaction pathway and key structures involved in the loss of $HN{=}CHCO_2H$ from protonated 2-oxo-histidine. All energies are listed as relative $\Delta G_{298}$ to **09a** (in kcal.mol$^{-1}$), with the structures optimised at the B3-LYP/6-311++G(d,p) level.



DOI: 10.1002/rcm

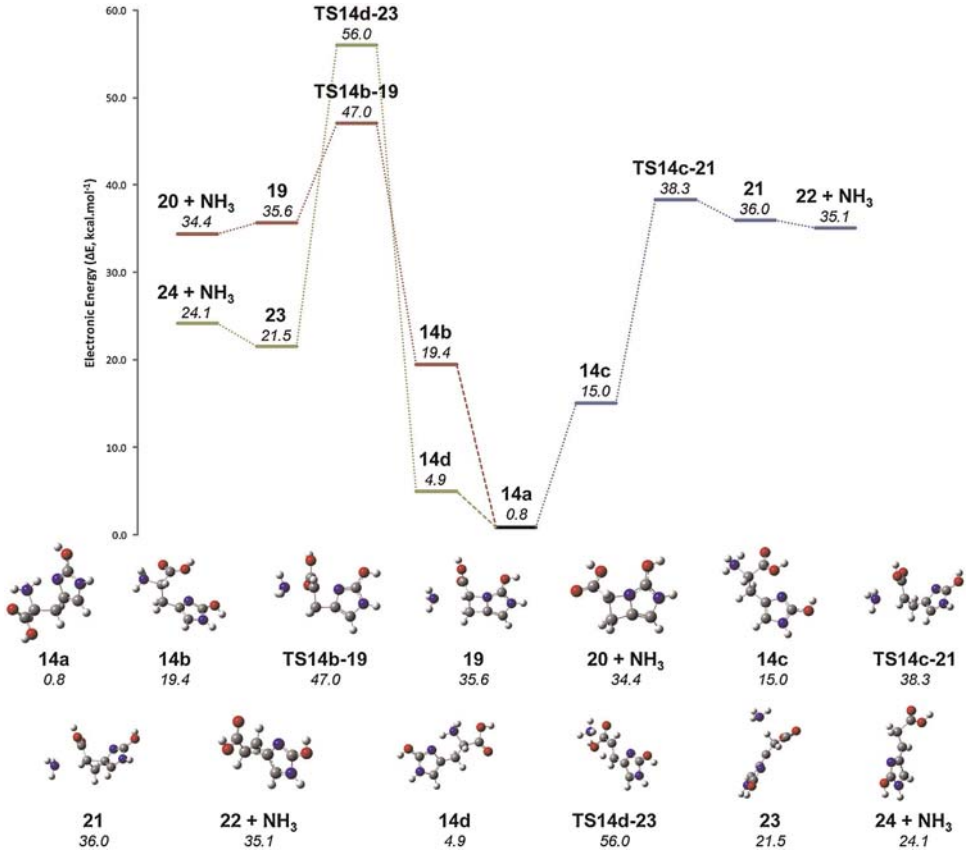


**Figure 6.** Calculated reaction pathways and key structures involved in the loss of $NH_3$ from protonated 2-oxo-histidine via (a) formation of a four-membered ring (red); (b) formation of a three-membered ring (blue); and (c) 1,2 hydride migration (green). All energies are listed as relative $\Delta G_{298}$ to **09a** (in kcal.mol$^{-1}$), with the structures optimised at the B3-LYP/6-311++G(d,p) level.

## Fragmentation mechanisms for MS/MS dissociation of protonated 2-oxo-histidine (Fig. 2(A))

### *Losses of $H_2O$, CO from protonated 2-oxo-histidine (Eqns. (1) and (2))*

Figure 4 shows the PES for the stepwise loss of neutral water and carbon monoxide from protonated 2-oxo-histidine. Attempts to locate a transition state by modelling a concerted mechanism for the loss of $H_2O$, CO – analogous to that found for protonated cysteine[49] – were unsuccessful. The loss of $H_2O$ and CO to yield the $a_1$ ion **13** is proposed to occur via a concerted process in which the ionising proton is transferred from $N_\pi$ onto the hydroxyl group, thereby allowing for nucleophilic attack by the imino nitrogen on the side chain onto the carbonyl. The barrier against this dissociation is 39.2 kcal.mol$^{-1}$ (**TS09b-10**) relative to **09a** to yield the ion-molecule complex **10**, which upon separation yields **11** which is 13.0 kcal.mol$^{-1}$ higher in energy than **09a**. The subsequent loss of neutral CO directly from **11** occurs via **TS11-12** to finally give the $a_1$ ion **13** which has an endoergicity of 5.5 kcal.mol$^{-1}$.

### *Loss of HN=CHCO$_2$H from protonated 2-oxo-histidine (Eqn. (7))*

Figure 5 shows the PES for loss of the imine HN=CHCO$_2$H from protonated 2-oxo-histidine while Scheme 6 highlights the key steps involved. Attempts to locate a transition state in which a hydrogen atom is shifted from the $N_\pi$ nitrogen to the C5 carbon were unsuccessful. Instead an indirect route was obtained in which the proton first migrated away from the side chain then transferred back onto the desired atom (Scheme 6). This series of intramolecular proton transfer reactions starts when the proton migrates from $N_\pi$ to the amino group, a process with a very modest barrier of 1.1 kcal.mol$^{-1}$ above **09a** (**TS09a-14a**). From the resultant ion **14a**, the diol **15a** is formed, a process occurring via **TS14a-15a** (18.3 kcal.mol$^{-1}$ above **09a**). The required carbocation **16** is formed from **15b** via **TS15b-16**, which is 1.0 kcal.mol$^{-1}$ higher in energy than **15b**. The subsequent dissociation of **16** occurs via transition state **TS16-17** which has a barrier of 33.3 kcal.mol$^{-1}$ above **09a** to yield the ion-molecule complex **17**, which upon separation results in **18**, with an overall endoergicity of 22.1 kcal.mol$^{-1}$.

### *Loss of $NH_3$ from protonated 2-oxo-histidine (Eqn. (4))*

The loss of neutral ammonia can occur via one of three potential mechanisms as shown in Scheme 7. These are: (i) nucleophilic attack by the side-chain $N_\pi$ on the alpha-carbon to form an azetidine containing a bicyclic structure – pathway A; (ii) nucleophilic attack by the $N_\tau$ on the imidazole ring onto the adjacent C3 carbon resulting in the formation of a spiro product – pathway B; and (iii) pathway C – loss via a 1,2-hydride shift process. The PES for the three possible mechanistic pathways for the loss of $NH_3$ are shown in Fig. 6.



DOI: 10.1002/rcm

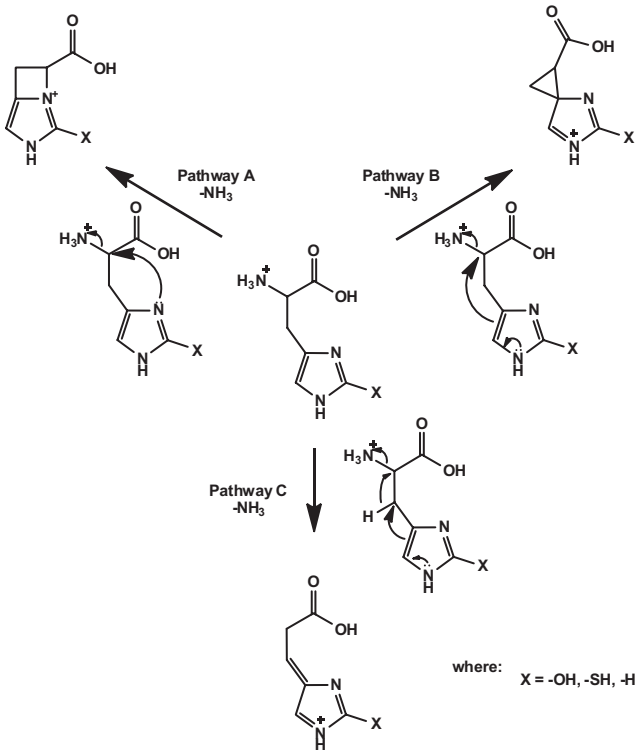


**Scheme 7.**

Loss of neutral ammonia from the N-terminus of **14a** to yield the bicyclic species **20** is predicted to occur via conformer **14b**, which is 19.4 kcal.mol$^{-1}$ higher in energy than **09a** (Fig. 6). The dissociation proceeds through transition state **TS14b-19** (47.0 kcal.mol$^{-1}$ relative to **09a**). Separation of the ion-molecule complex **19** leads to the product **20**, which lies 34.4 kcal.mol$^{-1}$ higher in energy than **09a**. The barrier against $NH_3$ loss via this mechanism is higher than the competing pathway B, suggesting that loss of $NH_3$ does not occur via this process.

Loss of $NH_3$ via pathway B occurs via the transition state **TS14c-21** to yield **21**, with the barrier against this process being 38.3 kcal.mol$^{-1}$. The resultant ion-molecule complex is 36.0 kcal.mol$^{-1}$ higher in energy than **09a**, and upon separation yields the ion **22** which has an endoergicity of 35.1 kcal.mol$^{-1}$. As the energy against this transition state is the lowest of the three proposed pathways, the ion at $m/z$ 155 is predicted to occur via this mechanism.

The final potential pathway, pathway C, is predicted to occur via conformer **14d**, with the dissociation taking place through transition state **TS14d-23** which lies 51.1 kcal.mol$^{-1}$ higher in energy than the neighbouring **14d**. Separation of the resulting ion-molecule complex **23** yields the ion **24**. The substantial barrier associated with the transition state from this pathway indicates that loss of $NH_3$ is unlikely is occur through this pathway. Interestingly, the product that results from this transition state, **TS14d-23**, has the lowest endoergicity with a value of 24.1 kcal.mol$^{-1}$. This further highlights that low-energy CID reactions are under kinetic rather than thermodynamic control.

## Fragmentation mechanisms for MS/MS dissociation of protonated 2-thioxo-histidine and histidine

As the PES of both 2-thioxo-histidine and protonated histidine are similar to that of 2-oxo-histidine, with analogous transitions states differing only in their relative stabilities, the energies associated with the crucial barriers against the various dissociations are summarised in Table 3. The PES of 2-thioxo-histidine and histidine, with their respective Cartesian coordinates, can be found in the Supporting Information.

From an examination of Table 3 the following conclusions can be reached:

i. There is an excellent correlation between the ions observed experimentally (Fig. 2) and the barriers against the key transition states for the three losses;
ii. Whilst the barriers against loss of water and the subsequent loss of CO remain largely unchanged (Eqns. (1) and (2)), the introduction of an alcohol or thiol group onto the imidazole side chain dramatically lowers the barriers against $NH_3$ loss via the most thermodynamically favoured process (Eqn. (4b));
iii. The loss of $[C_2,H_3,O_2,N]$ is observed in the MS/MS spectra of protonated 2-oxo- and 2-thioxo-histidine (Figs. 2(B) and 2(C)) yet is not observed for protonated histidine (Fig. 2(C)) as the barriers against loss of $HN{=}CHCO_2H$ are lowered by the introduction of the carbonyl and thiocarbonyl moieties;
iv. Regarding the reduced nucleophilicity reported for the dissociation of peptides containing oxidised histidine residues,[18] the introduction of an oxygen or sulfur atom onto the 2-position of the imidazole side chain appears to affect the nucleophilicity of $N_\pi$ in ways that are dependent on the type of reaction. The barrier for neighbouring group attack via this atom to lose water (Eqn. (2)) is slightly raised, whereas loss of ammonia via pathway A

**Table 3.** Summary of the barriers against the key transition states involved in the $H_2O$; $H_2O$, CO; $HN{=}CHCO_2H$; and $NH_3$ fragmentation pathways. The numbers in parentheses correspond to the final endoergicities for the products following separation of the ion-molecule complex. All energies are listed as relative $\Delta G_{298}$ to their most stable protonated conformer, **09a**, **M09a** and **H09a** (in kcal.mol$^{-1}$), with the structures optimised at the B3-LYP/6-311++G(d,p) level

| | | Histidine species | | |
|---|---|---|---|---|
| Eqn. | Dissociation | 2-oxo-histidine | 2-thioxo-histidine | histidine |
| (2) | $H_2O$ | 39.2 (13.0) | 38.6 (15.1) | 38.3 (15.8) |
| (1) | $H_2O$, CO | 33.4 (5.5) | 35.3 (5.6) | 35.2 (4.8) |
| (7) | $HN{=}CHCO_2H$ | 33.3 (22.1) | 38.4 (24.2) | 42.3 (27.5) |
| (4a) | $NH_3$ (pathway A) | 47.0 (34.4) | 45.9 (32.9) | 45.4 (32.9) |
| (4b) | $NH_3$ (pathway B) | 38.3 (35.1) | 42.2 (39.2) | 44.3 (42.1) |
| (4c) | $NH_3$ (pathway C) | 56.0 (24.1) | 55.1 (22.8) | Not Found |





DOI: 10.1002/rcm

(Eqn. (4a)) is slightly decreased for the two modified histidine derivatives.

## CONCLUSIONS

Introduction of an oxygen or sulfur atom onto the side chain of histidine was found to have a significant effect on the gas-phase properties of the amino acid, altering the preferred tautomer to the keto, **2c**, and thioketo, **3c**, forms, thereby lowering their proton affinities. These changes in turn influence the fragmentation chemistry of the modified histidine residues. The change in fragmentation for the protonated amino acids is subtle, with protonated **2** and **3** undergoing additional minor losses of $NH_3$ and the imine HN=$CHCO_2H$. Introduction of a methyl ester enhances the difference in fragmentation chemistry, which appears to be amplified in larger peptides whereby the preferential cleavage C-terminal to the histidine residue[18] is suppressed for 2-oxo-histidine residues. Since recent studies have indicated that oxidised histidine residues can be correctly assigned using electron-transfer dissociation, ETD,[50] future studies will explore the gas-phase chemistry of 2-oxo- and 2-thioxo-histidine radical cations.

## SUPPORTING INFORMATION

Additional supporting information may be found in the online version of this article.

### Acknowledgements

We thank the ARC for financial support via the ARC Centre of Excellence in Free Radical Chemistry and Biotechnology. The authors gratefully acknowledge the generous allocation of computing time from both the Victorian Partnership for Advanced Computing and the NCI National Facility. The authors would also like to thank the ARC and VICS for funding of the LTQ FT hybrid mass spectrometer instrument. AKYL acknowledges the award of a Melbourne Research Scholarship from The University of Melbourne. The authors would also like to acknowledge discussions with Christopher K. Barlow and Brett Paterson, and Barbara Li for advice on the synthesis of 2-oxo-histidine.

## REFERENCES

1. Davies MJ. *Biochim. Biophys. Acta, Proteins Proteomics* 2005; **1703**: 93.
2. Wang Y, Vivekananda S, Men L, Zhang Q. *J. Am. Soc. Mass Spectrom.* 2004; **15**: 697.
3. Men L, Wang Y. *Rapid Commun. Mass Spectrom.* 2005; **19**: 23.
4. Kotiaho T, Eberlin MN, Vainiotalo P, Kostiainen R. *J. Am. Soc. Mass Spectrom.* 2000; **11**: 526.
5. Reid GE, Roberts KD, Kapp EA, Simpson RJ. *J. Proteome Res.* 2004; **3**: 751.
6. Vazquez S, Truscott RJW, O'Hair RAJ, Weimann A, Sheil MM. *J. Am. Soc. Mass Spectrom.* 2001; **12**: 786.
7. Lloyd JA, Spraggins JM, Johnston MV, Laskin J. *J. Am. Soc. Mass Spectrom.* 2006; **17**: 1289.
8. Spraggins JM, Lloyd JA, Johnston MV, Laskin J, Ridge DP. *J. Am. Soc. Mass Spectrom.* 2009; **20**: 1579.
9. Lioe H, O'Hair RAJ, Reid GE. *Rapid Commun. Mass Spectrom.* 2004; **18**: 978.
10. Ronsein GE, Bof deOliveira, Gennari MC, de Medeiros MH, Di Mascio P. *J. Am. Soc. Mass Spectrom.* 2009; **20**: 188.
11. Jiang X, Smith JB, Abraham EC. *J. Mass Spectrom.* 1996; **31**: 1309.
12. O'Hair RAJ, Reid GE. *Eur. Mass Spectrom.* 1999; **5**: 325.
13. Lioe H, Laskin J, Reid GE, O'Hair RAJ. *J. Phys. Chem. A* 2007; **111**: 10580.
14. Lewisch SA, Levine RL. *Anal. Biochem.* 1995; **231**: 440.
15. Hong V, Presolski SI, Ma C, Finn MG. *Angew. Chem., Int. Ed.* 2009; **48**: 9879, 9879/1.
16. Inoue K, Garner C, Ackermann BL, Oe T, Blair IA. *Rapid Commun. Mass Spectrom.* 2006; **20**: 911.
17. Schoneich C. *Exp. Gerontol.* 2006; **41**: 807.
18. Bridgewater JD, Srikanth R, Lim J, Vachet RW. *J. Am. Soc. Mass Spectrom.* 2007; **18**: 553.
19. Schoneich C. *J. Pharm. Biomed. Anal.* 2000; **21**: 1093.
20. Uchida K. Amino Acids. 2003; **25**: 249.
21. Uchida K, Kawakishi S. FEBS Lett. 1993; **332**: 208.
22. Uchida K, Kawakishi S. *J. Biol. Chem.* 1994; **269**: 2405.
23. Wysocki VH, Tsaprailis G, Smith LL, Breci LA. *J. Mass Spectrom.* 2000; **35**: 1399.
24. Farrugia JM, Taverner T, O'Hair RAJ. *Int. J. Mass Spectrom.* 2001; **209**: 99.
25. Farrugia JM, O'Hair RAJ, Reid GE. *Int. J. Mass Spectrom.* 2001; **210/211**: 71.
26. Tsaprailis G, Nair H, Zhong W, Kuppannan K, Futrell JH, Wysocki VH. *Anal. Chem.* 2004; **76**: 2083.
27. Furuta T, Katayama M, Shibasaki H, Kasuya Y. *J. Chem. Soc., Perkin Trans. 1: Org. Bio-Org. Chem.* 1992; 1643.
28. Hegedus B. *Helv. Chim. Acta* 1955; **38**: 22.
29. Levene PA. *Org. Synth.* 1943; **2**: 88.
30. Frisch MJ, Trucks GW, Schlegel HB, Scuseria GE, Robb MA, Cheeseman JR, Montgomery JA Jr, Vreven T, Kudin KN, Burant JC, Millam JM, Iyengar SS, Tomasi J, Barone V, Mennucci B, Cossi M, Scalmani G, Rega N, Petersson GA, Nakatsuji H, Hada M, Ehara M, Toyota K, Fukuda R, Hasegawa J, Ishida M, Nakajima T, Honda Y, Kitao O, Nakai H, Klene M, Li X, Knox JE, Hratchian HP, Cross JB, Bakken V, Adamo C, Jaramillo J, Gomperts R, Stratmann RE, Yazyev O, Austin AJ, Cammi R, Pomelli C, Ochterski JW, Ayala PY, Morokuma K, Voth GA, Salvador P, Dannenberg JJ, Zakrzewski VG, Dapprich S, Daniels AD, Strain MC, Farkas O, Malick DK, Rabuck AD, Raghavachari K, Foresman JB, Ortiz JV, Cui Q, Baboul AG, Clifford S, Cioslowski J, Stefanov BB, Liu G, Liashenko A, Piskorz P, Komaromi I, Martin RL, Fox DJ, Keith T, Al-Laham MA, Peng CY, Nanayakkara A, Challacombe M, Gill PMW, Johnson B, Chen W, Wong MW, Gonzalez C, Pople JA. *Gaussian 03, Revision B.04*. Gaussian Inc.: Wallingford, CT, 2004.
31. Becke AD. *J. Chem. Phys.* 1993; **98**: 5648.
32. Lee C, Yang W, Parr RG. *Phys. Rev. B: Condens. Matter Mater. Phys.* 1988; **37**: 785.
33. Gonzalez C, Schlegel HB. *J. Chem. Phys.* 1989; **90**: 2154.
34. Tawa GJ, Topol IA, Burt SK, Caldwell RA, Rashin AA. *J. Chem. Phys.* 1998; **109**: 4852.
35. Kovačević B, Rozman M, Klasinc L, Srzic D, Maksic ZB, Yanez M. *J. Phys. Chem. A* 2005; **109**: 8329.
36. Ellestad GA, Cosulich DB, Broschard RW, Martin JH, Kunstmann MP, Morton GO, Lancaster JE, Fulmor W, Lovell FM. *J. Am. Chem. Soc.* 1978; **100**: 2515.
37. Schubert G, Reck G, Jancke H, Kraus W, Patzelt C. *Urol. Res.* 2005; **33**: 231.
38. Ren Y, Li M, Wong N-B. *J. Mol. Model.* 2005; **11**: 167.
39. Lioe H, O'Hair RAJ, Gronert S, Austin A, Reid GE. *Int. J. Mass Spectrom.* 2007; **267**: 220.
40. McLuckey SA, Cameron D, Cooks RG. *J. Am. Chem. Soc.* 1981; **103**: 1313.
41. Cooks RG, Koskinen JT, Thomas PD. *J. Mass Spectrom.* 1999; **34**: 85.
42. Wu Z, Fenselau C. *Rapid Commun. Mass Spectrom.* 1994; **8**: 777.
43. Cerda BA, Hoyau S, Ohanessian G, Wesdemiotis C. *J. Am. Chem. Soc.* 1998; **120**: 2437.
44. Gronert S, Simpson DC, Conner KM. *J. Am. Soc. Mass Spectrom.* 2009; **20**: 2116.
45. Dinadayalane TC, Sastry GN, Leszczynski J. *Int. J. Quantum Chem.* 2006; **106**: 2920.
46. Harrison AG. *Mass Spectrom. Rev.* 1997; **16**: 201.
47. Hunter EPL, Lias SG. *J. Phys. Chem. Ref. Data* 1998; **27**: 413.
48. Reid GE, Simpson RJ, O'Hair RAJ. *J. Am. Soc. Mass Spectrom.* 1998; **9**: 945.
49. O'Hair RAJ, Styles ML, Reid GE. *J. Am. Soc. Mass Spectrom.* 1998; **9**: 1275.
50. Srikanth R, Wilson J, Vachet RW. *J. Mass Spectrom.* 2009; **44**: 755.





DOI: 10.1002/rcm